

1 **Temperature dependent Al-induced crystallization of amorphous Ge thin films on SiO<sub>2</sub>**  
2 **substrates**

3  
4 Kaoru Toko<sup>a</sup>, Naoki Fukata<sup>b</sup>, Koki Nakazawa<sup>a</sup>, Masashi Kurosawa<sup>c</sup>, Noritaka Usami<sup>d</sup>,  
5 Masanobu Miyao<sup>c</sup>, and Takashi Suemasu<sup>a</sup>

6  
7 <sup>a</sup> *Institute of Applied Physics, University of Tsukuba, Tsukuba, Ibaraki 305-8573, Japan*

8 <sup>b</sup> *National Institute for Materials Science, Namiki, Tsukuba, 305-0044, Japan*

9 <sup>c</sup> *Department of Electronics, Kyushu University, Motoooka, Fukuoka 819-0395, Japan*

10 <sup>d</sup> *Institute of Materials Research, Tohoku University, Sendai, Miyagi 980-8577, Japan*

11

12

13

14

15

16

17 *Keywords:* A1.Crystal orientation, A2.Solid phase crystallization, B1.Polycrystalline films;

18 B2.Semiconducting germanium

19

20 High-quality crystalline Ge thin-films on low-cost glass substrates are desired to reduce the  
21 fabrication cost of high-efficiency tandem solar cells. We applied an Al-induced  
22 crystallization technique to amorphous-Ge films (50-nm thickness) on SiO<sub>2</sub> glass substrates.  
23 The annealing temperature of the sample strongly influenced the grain size and the crystal  
24 orientation in the grown polycrystalline Ge layers: low annealing temperatures resulted in  
25 large grains and high (111)-orientation fractions. As a result, annealing at 325 °C provided  
26 98% (111)-oriented grains with average diameters of 30-μm. Moreover, the grown Ge layers  
27 could be used as an epitaxial template for chemical vapor deposition. This large-grained Ge  
28 film on a SiO<sub>2</sub> substrate appears promising for use as a Ge light-absorbing layer, as well as an  
29 epitaxial buffer layer for group III-V compound semiconductors.

30

## 31 **1. Introduction**

32 Germanium has been used in the bottom cell of high-efficiency tandem solar cells  
33 because of its desirable characteristics, such as its narrow band gap (0.66 eV), large  
34 absorption coefficient ( $\sim 10^4 \text{ cm}^{-1}$  at 1.1 eV), and good lattice matching to group III-V  
35 compound semiconductors (0.1% lattice mismatch with GaAs) [1]. However, bulk Ge  
36 substrates are extremely expensive, which has limited their application to special uses, such as  
37 in tandem solar cells for space satellites. One promising approach to reducing fabrication cost  
38 is substituting the bulk Ge substrate with a high-quality Ge thin film on a low-cost glass  
39 substrate. Here, a low-temperature process ( $< 550 \text{ }^\circ\text{C}$ ) is required to avoid softening the glass  
40 substrate. Considering the absorption coefficient of Ge, the optimum thickness of the Ge layer  
41 is calculated to be approximately 3- $\mu\text{m}$ . In order to be able to draw photoexcited carriers to  
42 the bottom and top electrodes, the grain size in the Ge layer should be larger than 3- $\mu\text{m}$  in  
43 diameter, because grain boundary scattering quenches the photoexcited carriers. Specifically,  
44 a polycrystalline Ge (poly-Ge) layer works almost as well as a single-crystal Ge substrate if  
45 the grain size is sufficiently large and the crystallinity of each grain is sufficiently high. A  
46 promising technique for forming large-grained group III-V compound semiconductors for the  
47 middle or top cells is epitaxial growth from each grain of the bottom Ge layer [2]. Regarding  
48 the crystal orientation, (111)-oriented Ge is favorable for forming nanowires, which  
49 dramatically enlarge the light-absorbing area [3, 4]. Many researchers have developed

50 advanced growth techniques: solid-phase crystallization (SPC) [5-7], metal-induced SPC  
51 [8-10], laser annealing [11-13], and chemical vapor deposition (CVD) [14]. However, the  
52 resulting Ge layers consist of small, submicron grains, with nearly random orientations.

53 Aluminum-induced crystallization (AIC) is a metal-induced SPC technique developed  
54 for amorphous-Si (a-Si) films on glass substrates [15-23]. CVD of Si layers onto the AIC-Si  
55 thin film is a promising approach to fabricating low-defect, large-grained Si layers on glass  
56 substrates [24, 25]. However, AIC of amorphous Ge (a-Ge) had been difficult to accomplish  
57 [26-29]. Recently, we realized Ge-AIC by preparing thin Ge and Al layers (50-nm thickness)  
58 and optimizing the thickness of the  $\text{AlO}_x$  interfacial layer (~1 nm) [30]. This resulted in  
59 preferentially (111)-oriented (~68%) poly-Ge films with relatively large-grains (5- $\mu\text{m}$   
60 diameters). In this paper, the (111)-orientation fraction and the grain size are dramatically  
61 improved by lowering the annealing temperature. Moreover, we demonstrate the usability of  
62 the Al-induced crystallized Ge (AIC-Ge) films as an epitaxial template for large-grained  
63 active Ge layers.

64

## 65 **2. Experimental procedure**

66 The preparation of the Al and Ge layers on quartz glass ( $\text{SiO}_2$ ) substrates was carried  
67 out at room temperature using a radio-frequency magnetron sputtering method. The  
68 deposition times were 2.5 minutes for Al and 2.2 minutes for Ge, respectively. Between the

69 two deposition cycles, the Al films were exposed to air for 5 minutes to form native  $\text{AlO}_x$   
70 layers, in order to form a diffusion control layer. The thicknesses of the Al and a-Ge layers  
71 were selected to be 50 nm each, because this thickness is favorable for the AIC growth of  
72 a-Ge [30]. Finally, the samples were annealed at 325-400 °C in  $\text{N}_2$  for 1-100 h. The surface  
73 morphologies of the Ge layers were observed by Nomarski optical microscopy and scanning  
74 electron microscopy (SEM). The Raman spectra were recorded using a Jobin Ivon Raman  
75 microprobe system, with an  $\text{Ar}^+$  laser (514.5 nm) excitation in a backscattering geometry.  
76  $\theta$ - $2\theta$  x-ray diffraction (XRD) measurements were performed using a Rigaku SmartLab system  
77 with a Ge monochromator at a wavelength of 1.54 Å. The grain size and crystal orientation  
78 were evaluated by electron backscattered diffraction (EBSD) measurement. Prior to the EBSD  
79 measurement, the aluminum and oxide layers on the Ge layers were etched using an HF  
80 solution (HF: 1.5%) for one minute.

81

### 82 **3. Results and Discussion**

83 Figs. 1(a) shows the expected schematic diagrams of the respective crystallization  
84 stages, that is, Ge diffusion into Al, Ge lateral growth, and layer exchange. Each diagram  
85 corresponds to its respective Nomarski optical micrograph in Fig. 1(b). These micrographs  
86 show the back surface of the sample observed through the transparent quartz substrate. The  
87 annealing temperature is 375 °C. These micrographs suggest that the Ge atoms diffuse to the

88 back surface, grow laterally, and cover the entire substrate during the annealing. The Raman  
89 spectra in Fig. 1(c) show the appearance of a large peak after annealing. This peak, at around  
90  $295\text{ cm}^{-1}$ , originates from the vibration mode of Ge-Ge bonds, indicating the crystallization of  
91 the Ge layer through the layer exchange process. These results typically demonstrate the  
92 completion of AIC of a-Ge on a quartz glass substrate.

93 The EBSD measurement statistically characterizes the crystal orientation of the AIC-Ge,  
94 as a function of the annealing temperature ( $400\text{ }^{\circ}\text{C}$ ,  $375\text{ }^{\circ}\text{C}$ ,  $350\text{ }^{\circ}\text{C}$ , and  $325\text{ }^{\circ}\text{C}$ ). The  
95 lower the annealing temperature, the longer the annealing time required for completion of the  
96 AIC: (a) 1 h ( $400\text{ }^{\circ}\text{C}$ ), (b) 10 h ( $375\text{ }^{\circ}\text{C}$ ), (c) 30 h ( $350\text{ }^{\circ}\text{C}$ ), and (d) 100 h ( $325\text{ }^{\circ}\text{C}$ ). The  
97 crystal orientation maps along the normal ( $z$ ) and in-plane ( $x$ ) directions relative to the sample  
98 surfaces are respectively shown in Figs. 2(a)-2(d) and Figs. 2(e)-2(h). We can estimate the  
99 grain size from the in-plane orientation maps, because the in-plane crystal directions are  
100 different among the respective grains. The orientation maps in Fig. 2 clearly indicate that the  
101 orientation and grain size of the AIC-Ge layers strongly depend on the annealing temperature:  
102 a lower annealing temperature results in a dominant (111) orientation and a larger grain size in  
103 the AIC-Ge layers.

104 The EBSD analysis is used to derive the area-fractions of the (111) orientation; the  
105 average grain size from the EBSD maps is shown in Figs. 2(a)-2(h). The result is shown in  
106 Fig. 3(a). By definition, the (111) fraction contains planes with tilt that is within  $10^{\circ}$  of the

107 exact (111) plane. Fig. 3(a) clearly indicates that both the (111) fraction and the grain size  
108 increase with decreasing annealing temperature. As a result, the (111) fraction is as high as  
109 98% and the grain size is as large as 30- $\mu\text{m}$  diameter for an annealing temperature of 325  $^{\circ}\text{C}$ .  
110 These values are the highest among those previously reported for poly-Ge layers on  
111 amorphous substrates in low-temperature processes [5-14]. In our previous work on AIC-Ge  
112 annealed at 410  $^{\circ}\text{C}$  [30], the (111) fraction and the grain size were limited to 68% and 5  $\mu\text{m}$ ,  
113 respectively. Therefore, we can conclude that lowering the annealing temperature is very  
114 important for enhancing the quality of the poly-Ge films in this AIC technique.

115         Next we discuss the annealing temperature dependence of the growth morphology. Ge  
116 nucleation models are illustrated in Fig. 3(b). In the AIC of Si, it has been reported that Si  
117 nucleation occurs when the Si concentration in the Al saturates at a level above the solubility  
118 limit [15,17,19,20]. In particular, Sarikov *et al.* clarified that the supersaturation level of Al  
119 with Si becomes higher when the annealing temperature is lowered [19]. This mechanism  
120 should be the same for the AIC of Ge. During annealing, Ge atoms gradually diffuse into the  
121 Al layer through the interfacial  $\text{AlO}_x$  layer. When the supersaturation level is low, the Ge  
122 concentration saturates in the bulk Al before the Ge atoms reach the  $\text{SiO}_2$  surface. Because Ge  
123 nucleation occurs homogeneously in the bulk Al, the orientation becomes random as shown in  
124 Fig. 3(b). In contrast, when the supersaturation level is high, Ge atoms can reach the  $\text{SiO}_2$   
125 surface without supersaturation occurring, and without homogeneous nucleation occurring in

126 the bulk Al. In the case of heterogeneous nucleation, the interfacial energy determines the  
127 preferential orientation of the nuclei [19, 31]. Because the (111) plane has the lowest  
128 interfacial energy in the diamond structure, (111)-oriented Ge nucleation occurs  
129 heterogeneously on the SiO<sub>2</sub> surface [32]. Therefore, the preference for the (111) orientation  
130 increases as the annealing temperature decreases. For the AIC technique, the initial nucleation  
131 density determines the grain size because lateral growth stops when the growth fronts collide  
132 [20]. Because a higher supersaturation level causes a lower nucleation rate [17,19], using a  
133 low annealing temperature results in a large-grained poly-Ge film.

134 We investigated epitaxial thickening of Ge on the AIC-Ge (grown at 350 °C) using the  
135 CVD technique to confirm that this AIC-Ge can be used as an epitaxial template for advanced  
136 materials and nanowires. In the CVD, we employed a GeH<sub>4</sub> gas source and kept the sample  
137 substrate at 450 °C. A 200-nm thick Ge layer was grown on the AIC-Ge film. The SEM and  
138 EBSD images of the CVD-thickened sample surface are shown in Figs. 4(a) and 4(b),  
139 respectively. The CVD layer clearly shows predominantly (111) orientation. This result  
140 indicates CVD epitaxial growth of the Ge layer on the AIC-Ge film, because conventional  
141 CVD-Ge layers without AIC-Ge templates consist of small grains with random orientations  
142 [14].

143 XRD measurements are performed to evaluate the epitaxial relationship between the  
144 CVD-Ge and AIC-Ge layers. Fig. 5(a) shows the XRD patterns taken from  $\theta$ - $2\theta$

145 measurements for the samples before and after CVD thickening. In both patterns, sharp peaks  
146 are observed at around  $27^\circ$ , which corresponds to the Ge (111) plane. This figure clearly  
147 shows that the CVD thickening strongly enlarges the Ge (111) peak, and other peaks do not  
148 appear. A reciprocal space map was obtained around the Ge (111) plane and is shown in Fig.  
149 5(b). A wide contour is observed in the reciprocal space map, which reflects the tilted (111)  
150 planes. The maximum tilt angle is calculated to be 12 degrees. This contour has only a single  
151 peak, which suggests that the orientation of the AIC-Ge and CVD-Ge layers is the same, due  
152 to homoepitaxial growth. The lattice constant of the Ge layer is calculated to be  $5.658 \text{ \AA}$  from  
153 the peak position, a value that is almost the same as the relaxed Ge lattice constant ( $5.66 \text{ \AA}$ ).  
154 Therefore, we have demonstrated the usability of this AIC-Ge thin film on an insulator as an  
155 epitaxial template for the CVD-Ge layer. It is expected that epitaxial growth of other  
156 advanced materials and unidirectionally aligned nanowires is possible using this technique.

157

#### 158 **4. Conclusions**

159 We have investigated the Al-induced crystallization (AIC) of an a-Ge film (50-nm  
160 thickness) on an insulator. The crystallization of the a-Ge layer occurred through the  
161 layer-exchange process. We found that the annealing temperature of the sample strongly  
162 influenced the grain size and crystal orientation in the grown Ge layers: a lower annealing  
163 temperature yielded larger grains and a higher (111)-orientation fraction. Annealing at  $325^\circ \text{C}$

164 increased the grain size to up to 30- $\mu\text{m}$  in diameter and the (111)-orientation fraction to up to  
165 98%. Moreover, the grown Ge layers proved suitable for use as an epitaxial template for  
166 chemical vapor deposition (CVD). This large-grained Ge layer on an insulator holds promise  
167 for use as a Ge light-absorbing layer and as an epitaxial buffer layer, not only for group III-V  
168 compound semiconductors, but also for nanowires and other advanced materials.

169

## 170 **Acknowledgements**

171 This work was partially supported by a Grant-in-Aid for Scientific Research from the  
172 Ministry of Education, Culture, Sport, Science, and Technology in Japan.

173

174 **References**

- 175 [1] R.R. King, D.C. Law, K.M. Edmondson, C.M. Fetzer, G.S. Kinsey, H. Yoon, R.A. Sherif,  
176 N.H. Karam, *Appl. Phys. Lett.* **90** (2007) 183516.
- 177 [2] M.G. Mauk, J.R. Balliet, B.W. Feyock, *J. Cryst. Growth* **250** (2003) 50.
- 178 [3] N. Fukata, K. Sato, M. Mitome, Y. Bando, T. Sekiguchi, M. Kirkham, J. I. Hong, Z. L.  
179 Wang, R. L. Snyder, *ACS Nano* **4** (2010) 3807.
- 180 [4] E.P. M. Bakkers, J. van Dam, S. De Franceschi, L.P. Kouwenhoven, M. Kaiser, M.  
181 Verheijen, H. Wondergem, P. van der Sluis, *Nature Materials* **3** (2004) 769.
- 182 [5] C.Y. Tsao, J.W. Weber, P. Campbell, P.I. Widenborg, D. Song, M.A. Green, *Appl. Surf. Sci.*  
183 **255** (2009) 7028.
- 184 [6] A.F. Khan, M. Mehmood, A.M. Rana, T. Muhammad, *Appl. Surf. Sci.* **256** (2010) 2031.
- 185 [7] K. Toko, I. Nakao, T. Sadoh, T. Noguchi, M. Miyao, *Solid-State Electron.* **53** (2009) 1159.
- 186 [8] H. Kanno, K. Toko, T. Sadoh, M. Miyao, *Appl. Phys. Lett.* **89** (2006) 182120.
- 187 [9] J.H. Park, P. Kapur, K.C. Saraswat, H. Peng, *Appl. Phys. Lett.* **91** (2007) 143107.
- 188 [10] K. Toko, H. Kanno, A. Kenjo, T. Sadoh, T. Asano, M. Miyao, *Appl. Phys. Lett.* **91** (2007)  
189 042111.
- 190 [11] H. Watakabe, T. Sameshima, H. Kanno, M. Miyao, *Thin Solid Films* **508** (2006) 315.
- 191 [12] W. Yeh, H. Chen, H. Huang, C. Hsiao, J. Jeng, *Appl. Phys. Lett.* **93** (2008) 094103.
- 192 [13] K. Sakaike, S. Higashi, H. Murakami, S. Miyazaki, *Thin Solid Films* **516** (2008) 3595.

- 193 [14] M. Tada, J.H. Park, J.R. Jain, K.C. Saraswat, J. Electrochem. Soc. **156** (2009) D23.
- 194 [15] O. Nast, T. Puzzer, L.M. Koschier, A.B. Sproul, S.R. Wenham, Appl. Phys. Lett. **73**  
195 (1998) 3214.
- 196 [16] Y. Sugimoto, N. Takata, T. Hirota, K. Ikeda, F. Yoshida, H. Nakashima, H. Nakashima,  
197 Jpn. J. Appl. Phys. **44** (2005) 4770.
- 198 [17] J. Schneider, A. Sarikov, J. Klein, M. Muske, I. Sieber, T. Quinn, H.S. Reehal, S. Gall, W.  
199 Fuhs, J. Cryst. Growth **287** (2006) 423.
- 200 [18] J.Y. Wang, Z.M. Wang, and E.J. Mittemeijer, J. Appl. Phys. **102** (2007) 113523.
- 201 [19] A. Sarikov, J. Schneider, J. Berghold, M. Muske, I. Sieber, S. Gall, W. Fuhs, J. Appl.  
202 Phys. **107** (2010) 114318.
- 203 [20] B.I. Birajdar, T. Antesberger, B. Butz, M. Stutzmann, E. Spiecker, Scripta Materialia **66**  
204 (2012) 550.
- 205 [21] M. Kurosawa, N. Kawabata, T. Sadoh, M. Miyao, Appl. Phys. Lett. **95** (2009) 132103.
- 206 [22] M. Jung, A. Okada, T. Saito, T. Suemasu, N. Usami, Appl. Phys. Express **3** (2010)  
207 095803.
- 208 [23] M. Kurosawa, K. Toko, N. Kawabata, T. Sadoh, M. Miyao, Solid-State Electron. **60**  
209 (2011) 7.
- 210 [24] I. Gordon, L. Carnel, D.V. Gestel, G. Beaucarne, J. Poortmans, Thin Solid Films **516**  
211 (2008) 6984.

- 212 [25] B.R. Wu, S.Y. Lo, D.S. Wu, S.L. Ou, H.Y. Mao, J.H. Wang, R.H. Horng, *Thin Solid*  
213 *Films* **520** (2012) 5860.
- 214 [26] F. Katsuki, K. Hanafusa, M. Yonemura, T. Koyama, M. Doi, *J. Appl. Phys.* **89** (2001)  
215 4643.
- 216 [27] S. Hu, A.F. Marshall, P.C. McIntyre, *Appl. Phys. Lett.* **97** (2010) 082104.
- 217 [28] Z. Wang, J. Wang, L. Jeurgens, E. Mittemeijer, *Phys. Rev. B* **77** (2008) 1.
- 218 [29] S. Peng, D. Hu, D. He, *Appl. Surf. Sci.* **258** (2012) 6003.
- 219 [30] M. Kurosawa, N. Kawabata, T. Sadoh, M. Miyao, *ECS J. Solid State Sci. and Tech.* **1**  
220 (2012) 144.
- 221 [31] C. Spinella, S. Lombardo, F. Priolo, *J. Appl. Phys.* **84** (1998) 5383.
- 222 [32] A.A. Stekolnikov, J. Furthmuller, F. Bechstedt, *Phys. Rev. B* **65** (2002) 115318.

223 **Fig. 1.** (a) Schematic structures of the expected growth stage during AIC of a-Ge. (b)  
224 Nomarski optical micrographs of the back surface of the sample annealed at 375 °C for 0 h, 2  
225 h, and 10 h. (c) Raman spectra before and after annealing. The peak at 295 cm<sup>-1</sup> corresponds  
226 to the Ge-Ge vibration mode.

227

228 **Fig. 2.** EBSD images of the AIC-Ge surfaces after annealing at 400 °C, 375 °C, 350 °C,  
229 and 325 °C. (a)-(d) normal (z) and (e)-(h) in-plane (x) directions with respect to the sample  
230 surface. The colors indicate the crystal orientation, according to the inserted color keys.

231

232 **Fig. 3.** (a) The (111)-orientation area-fraction and grain size of the AIC-Ge layers as a  
233 function of the annealing time. (b) Schematic model of the temperature-dependent  
234 (111)-orientation fraction and grain size: (111)-oriented nuclei are generated at the Ge/SiO<sub>2</sub>  
235 interface.

236

237 **Fig. 4.** (a) SEM and (b) EBSD images of the thickened Ge layer grown on the AIC-Ge  
238 template.

239

240 **Fig. 5.** XRD characterization of the thickened Ge layer grown on the AIC-Ge template. (a)  
241 XRD patterns obtained by  $\theta$ - $2\theta$  measurements before and after CVD-thickening and (b)

242 reciprocal space mapping taken around the Ge (111) reflection.

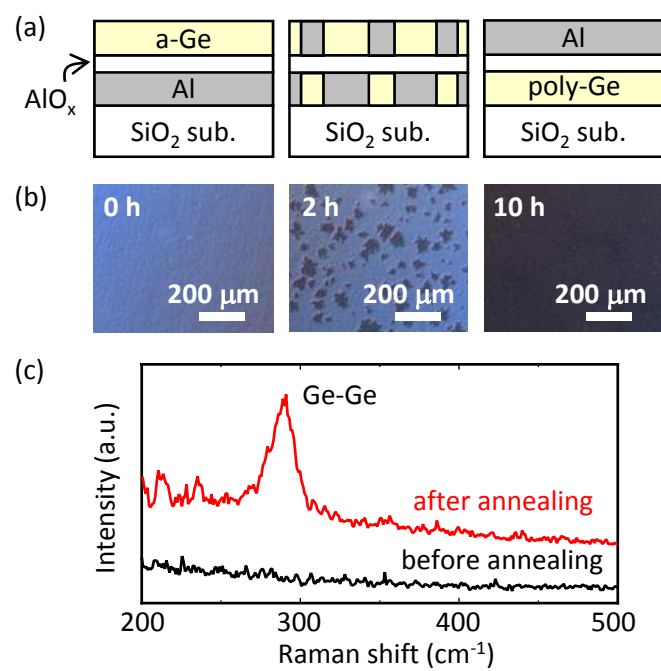


Figure 1 K. Toko

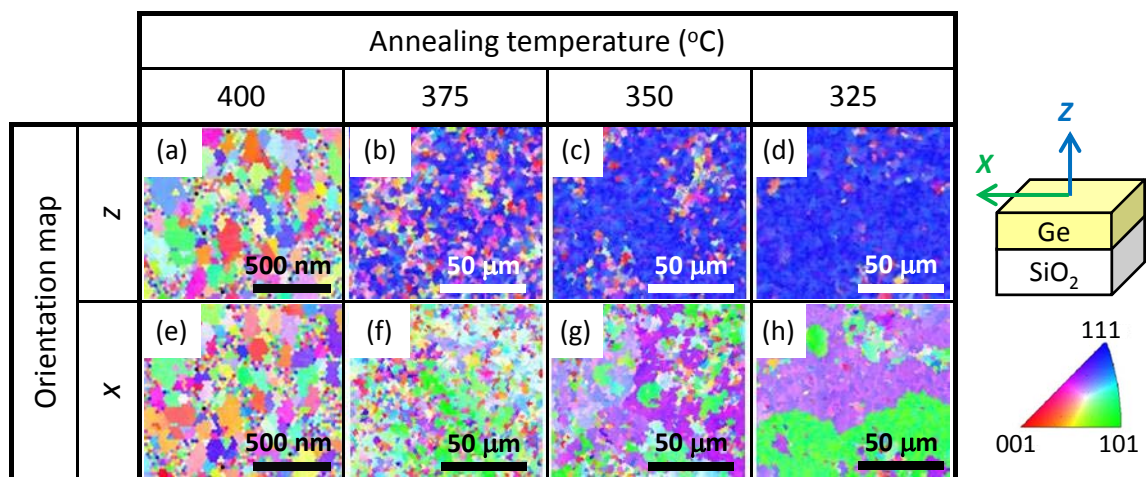


Figure 2 K. Toko

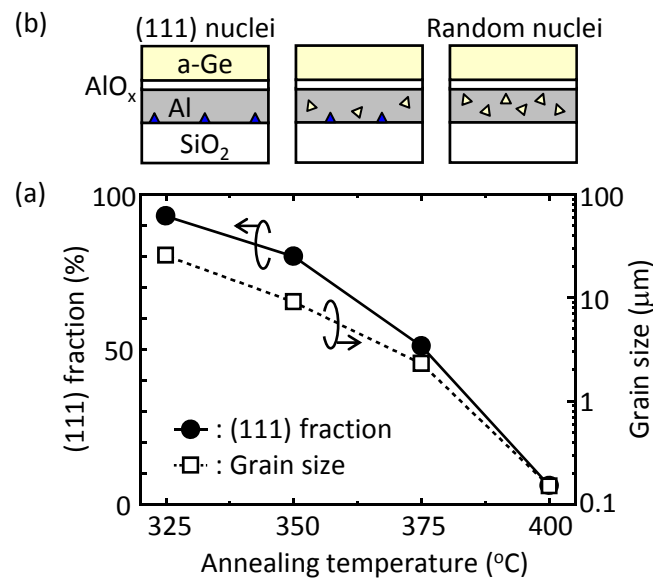
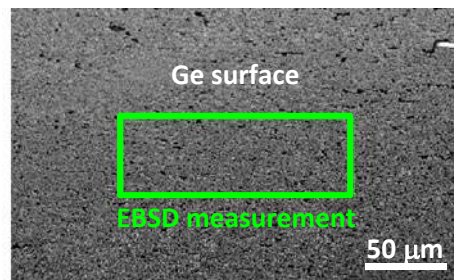


Figure 3 K. Toko

(a)



(b)

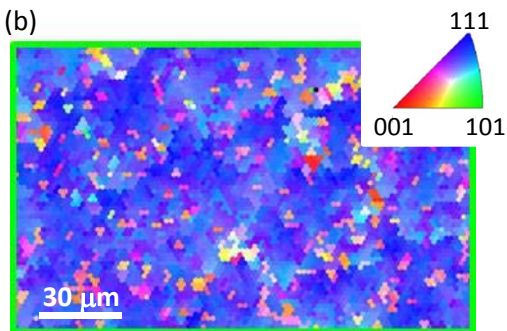


Figure 4 K. Toko

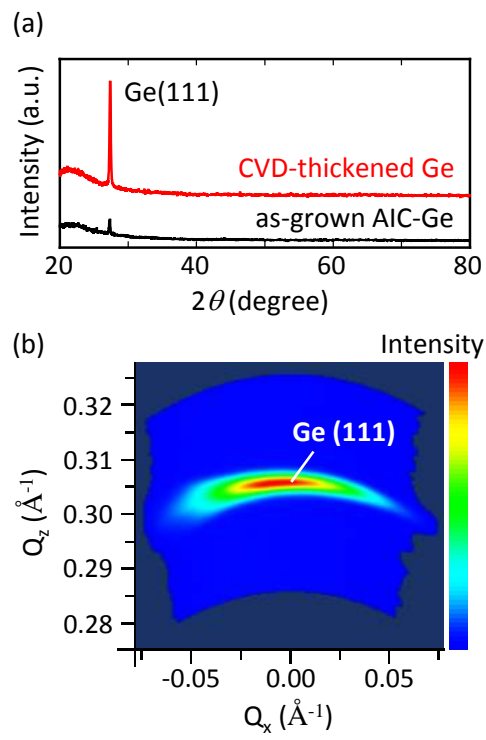


Figure 5 K. Toko